Nematic Order Drives Phase Separation in Polydisperse Liquid Crystalline Polymers

F. Elias, S. M. Clarke, R. Peck, and E. M. Terentjev*

Cavendish Laboratory, University of Cambridge, Madingley Road, Cambridge CB3 0HE, U.K.

ABSTRACT: In a polydisperse thermotropic main-chain liquid crystalline polymer, we observe the process of thermally induced nematic–nematic phase separation between short and long polymer chains. We study the dynamical features of this system, in particular the evolution of Schlieren textures formed by disclinations surrounding areas of relatively uniform director. We analyze the dependence of domain size ξ on temperature and the nematic order parameter, and the evolution of textures with the waiting time at a temperature well below the nematic transition T_{ni}. We find that before phase separation the coarsening proceeds toward the uniform state, with characteristic size of the texture increasing as $\xi \sim t^{1/4}$. When the system is phase-separated, the texture in the regions with long chains is frozen at an equilibrium value ξ, a reversible function of temperature, while in the short-chain regions the coarsening accelerates. This behavior is interpreted in terms of a miscibility gap that is proportional to the degree of nematic order, which is different for the different lengths of the nematic polymers.

1. Introduction

Schlieren textures in nematic liquid crystals[1] are due to the spatial variations of the director field $\mathbf{n}(\mathbf{r})$. They are visualized through the optical contrast between the birefringent regions with different orientations of this axis. A typical Schlieren texture has a variety of topological defects of the orientational order (disclinations) that match the director field between the domains with different orientation of $\mathbf{n}$. The average distance between disclinations represents the size of such correlated regions, within which the nematic director is more or less aligned, and is a characteristic length scale of the texture. Although there is no abrupt boundary separating such regions with different average director alignments, they are often referred to as domains, the average distance between disclinations being called the domain size ξ.

The presence of a texture in the director field is energetically unfavorable and is penalized in the nematic by the Frank elastic energy density $\sim \frac{1}{2}K(\nabla\mathbf{n})^2$.[1] As a result, if unconstrained, the textures always tend to relax toward the equilibrium uniform director alignment. Such a process is often viewed as the growth of correlated domains, or of the average distance between disclinations: the coarsening of the characteristic length scale $\xi(t)$. The evolution of nematic textures has been the subject of extensive research and interesting analogies.[2] Theoretical, as well as experimental, results of this research describe the interaction of disclinations of opposite sign, annihilating each other as the system approaches its lowest elastic energy equilibrium. The argument for such a law is simple[3,4] and based on representing a disclination as a line under tension τ. Assuming the texture is characterized by a single length scale ξ, the disclination line density should then scale as $\rho \sim \xi^{-2}$. Balancing the tension force per unit length, τ/ξ, against the viscous friction force, ηv, one finds the characteristic velocity of disclination movement $v = \tau/\eta\xi$. The rate of energy loss per unit volume is then $\dot{W} = \rho v \tau/\xi$ and is equal to the reduction in elastic tension energy density $\mathrm{d}/\mathrm{d}t(\rho\tau)$. One thus obtains the line density $\rho \sim (\eta/\tau)t^{-1}$, or the characteristic size of coarsening domain texture $\xi \sim t^{1/2}$.

Evidently, the dynamics of coarsening is determined by the laws of friction applied, for instance, to moving disclinations. Hence, the high viscosity (and, perhaps even more relevant—viscoelasticity) of liquid crystalline polymers (LCP) should make the coarsening of Schlieren textures much slower than that in low-molecular weight nematics. Indeed, this has been seen in many materials, particularly side-chain LCPs (see, for instance, ref 5), where the reorientation of mesogenic groups is restricted by connection to the polymer backbone. In main-chain liquid crystalline polymers (MCLCP), rodlike mesogenic groups separated by flexible spacers form the chains. In this case, the nematic director rotation is determined by the dynamics of polymer backbone itself.[6,7] The Schlieren textures in MCLCP and, in particular, the process of texture coarsening have been extensively studied over recent years.[8–12] It appears that the coarsening occurs via the annihilation of disclinations of opposite sign, as in other nematic systems. It has been reported that the average domain size scales as $\xi \sim t^{0.35}$,[10,11] noticeably slower than in a liquid nematic discussed above. However, in all MCLCPs studied, the textures seem to evolve toward a stable pattern, which is far from a uniform director that may have been expected to be the equilibrium. In other words, the characteristic domain size initially increases, as the coarsening dynamics would require, but then it appears to saturate at a constant value, of order of several micrometers,[12] In a previous study,[13] we have shown that in a MCLCP of high molecular weight, this final texture is an equilibrium state of the system, the domain size being a reversible function of the temperature. Such behavior is similar to the case of nematic elastomers, where the chains are permanently cross-linked in the network (see the review in ref 14 for details). There, the polydomain texture has been shown to represent a thermodynamic equilibrium in which the demand to minimize the Frank elastic energy is balanced by the quenched random-anisotropy effect of network cross-links.[15] It has been shown[16] that the characteristic domain size ξ is a reversible function of temperature, increasing toward the isotropic phase, $T \to T_{ni}$. In the case of non-cross-linked MCLCP, we have attributed the existence of equilibrium textures to the
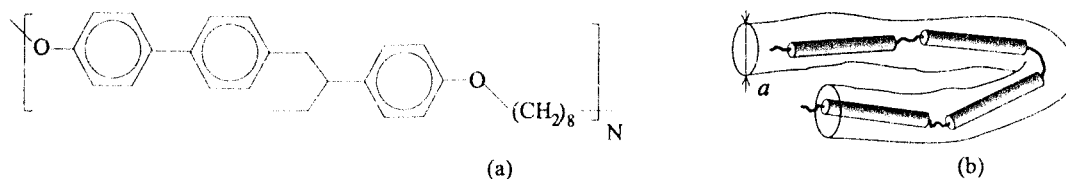
(a) (b)

Figure 1. (a) Chemical structure of a repeat unit of the liquid crystalline polymer used in this study. The rigid-rod mesogenic unit is 1-(4-hydroxy-4-biphenyl)-2-(4-hydroxyphenyl)butane, a rodlike object with length $l \approx 31$ Å. These groups are connected together to make a polymeric chain via flexible $(CH_2)_8$ spacers. (b) The sketch of main-chain liquid crystalline polymer of rigid-rod units connected by flexible spacers. The chain is confined in the reptation tube of diameter a, a function of chain contour length Nl. In the nematic phase, if a hairpin defect is created, the chain reptation may seize altogether, creating an effectively quenched source of orientational disorder. The average concentration of such sources is a function of nematic order parameter $Q(T)$.

presence of long-chain entanglements, which always exist at a fixed concentration in polymers of high molecular weight. The entanglements act, like cross-links in nematic elastomers, as local sources of disorder, quenching some mesogens in a random orientation. The equilibrium texture is then due to the competition between the tendency toward nematic ordering and the fact that the long polymeric chains remain entangled in order to maximize their configurational entropy.

In this paper, we investigate the role of polydispersity in the molecular weight of the nematic polymer. We use the same MCLCP as in ref 13 but with shorter chains and higher polydispersity. The observed textures show that, after a long time spent in the nematic phase (but well above the glass-transition temperature), a phase separation occurs. Drops of fine Schlieren texture appear within a region of coarser texture. At the same time calorimetry shows that the nematic−isotropic transition splits into two transitions at slightly different temperatures and increasing separation. In order to understand the composition of both phases and the mechanism of phase separation, we investigate the properties of each phase and of the preseparated sample. We study the time evolution and the temperature evolution of the characteristic domain size ξ. The underlying idea is that the behavior of the Schlieren texture provides an indirect but straightforward way to obtain information on the sample composition. In a preseparated sample, the average domain size ξ scales with time as a power law, as in other coarsening liquid crystalline textures. When the phase separation occurs, the characteristic size of the texture stops evolving in time inside the fine-texture drops. This texture has then reached an equilibrium state; when varying the temperature near the nematic−isotropic transition, it behaves reversibly, like in the case of long MCLCP chains studied in ref 13. At the same time the regions outside these drops continue their coarsening process. Having eliminated the possibility of a phase separation induced by impurities, we discuss the possibility of segregation between chains of different molecular weight. It has been shown in a number of studies that nematic order induces phase separation in polymer−liquid crystal blends.[17−19] In our case, however, all the polymers are made of the same monomers. We argue that short chains, below the hairpin length, are more likely to behave as regular nematic liquid crystals, whereas long chains are more likely to remain entangled. That makes our polydisperse MCLCP somewhat similar to these well-studied polymer-dispersed liquid crystals. We then present a simple theoretical argument, based on the Flory−Huggins concept for polymer mixtures, which accounts in a coherent way for both the microscopy experiments and the calorimetry measurements.

2. Experimental Section

The thermotropic MCLCP used in this study is a polyether with the chemical structure given in Figure 1a. The material has been synthesized in our laboratory, following the procedure outlined by Percec et al.[20] The polymer chains obtained in this synthesis have molecular weight of $M_n = 7000$ (number average) and $M_w = 22\,000$ (weight average), determined by gel permeation chromatography (polystyrene standard) at the Melville Laboratory for Polymer Synthesis. This makes the average number of monomers on a chain ∼15 and a polydispersity of ∼3, a broad unimodal distribution. The phase sequence of this polymer includes a nematic phase.[20] Differential scanning calorimetry (DSC, Perkin-Elmer Pyris 1) was used to identify the phase behavior of these materials. In this way we obtain the glass-transition temperature of $T_g = 38$ °C and nematic-to-isotropic transition temperature of $T_{ni} \approx 105$ °C.

After careful elimination of solvent, the samples are prepared in the following way. For DSC experiments, the polymer is annealed for 1 h at 170 °C (well above T_{ni}) for the polymer chains to reach the equilibrium state before the experiment begins. For optical microscopy, the polymer melt is spread between two clean glass slides at a high temperature by strongly shearing the slides (the thickness of the layer varies from 5 to 15 μm depending on the sample). It is then annealed for 10−20 h at 170 °C and placed on a temperature-controlled stage.

In order to investigate the possible role of chemical impurities in the observed process of phase separation, we have prepared a series of samples deliberately doping them with a low molecular weight compound, butylated hydroxytoluene (BHT). BHT is, in fact, present as a byproduct compound during the polymerization and is soluble in the MCLCP matrix. We have used samples from the same preparation batch, where the initial BHT was removed and then readded at 1.75% and 3.45%. The results show no difference in behavior (apart from expected small shifts in all characteristic temperatures), which led us to the conclusion that the observed phase-separation phenomena are related to the polydisperse liquid crystalline polymer and not to chemical impurities.

The textures were observed using polarized optical microscopy (Zeiss Axioplan). The characteristic length scale of textures (the domain size ξ) is determined by an image analysis procedure based on the statistical distribution of dark and light regions evident under crossed polars, and their connectivity, as described in ref 13. The domains of uniform director appear as clear spots surrounded by black lines of rapid director reversal (which link the disclinations); their area is determined after setting the appropriate gray level threshold. The characteristic length scale ξ is the square root of the mean domain area. The images were video-recorded via a CCD camera and analyzed in real space.

3. Phase-Separation Morphology

After the sample had been annealed at a high temperature, it was rapidly cooled to a temperature $T_w = 80$ °C, below T_{ni} but well above the glass transition T_g. Waiting a very long time at this temperature, we
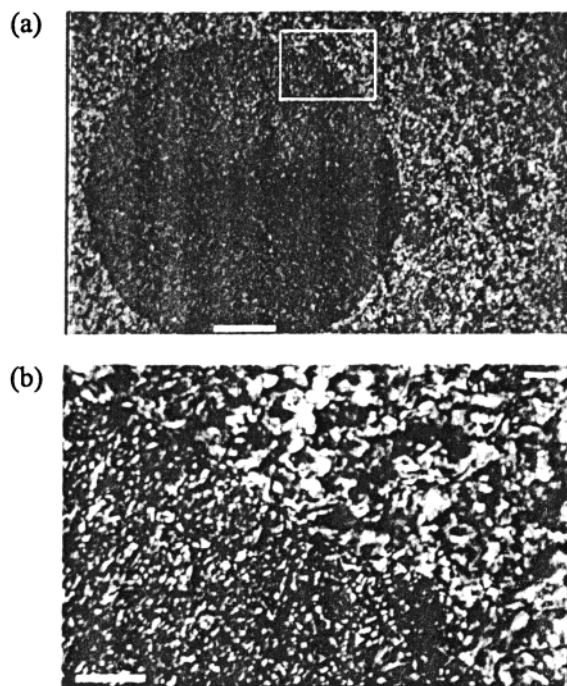
Figure 2. Micrographs of Schlieren textures in a MCLCP sample (film thickness $\simeq 10 \, \mu$m) between crossed polars, after 7500 min waiting at 80 °C, well above the glass-transition temperature but below the clearing point T_{ni}. In the image (a) two phases appear separated by a sharp interface: a circular drop of fine texture, within a continuous phase of coarser texture. The white bar represents 100 μm. Image (b) shows a higher magnification of domain interface segment (the white bar is 20 μm). The finer texture is the inside of the phase-separated drop in (a); the outside region has a significantly more coarsened texture with almost continuous regions of uniform director.

observed a phase separation in the sample. Figure 2 shows micrographs of the texture obtained when the sample was placed between crossed polars. Drops of fine texture appear within a region of coarser texture. The drops are circular and of macroscopic size, suggesting that the leading wavelength of phase separation is rather large. The interface between the two phases is sharp. On increasing the temperature, the nematic−isotropic transition proceeds in a different way inside and outside the phase-separated drops. Figure 3 shows image sequences of texture evolution on approaching T_{ni} in both regions. The temperature range of the transition is much broader in the outside region than inside the drops. Furthermore, the transition itself also seems qualitatively different: the change between nematic and isotropic regions appears clearly in the outside zone, whereas the transition seems more continuous inside the drops.

We have followed the thermal signature of phase separation using DSC measurements. Equilibration at a high temperature, well above T_{ni}, is required to ensure that no residual deformation of the polymer backbones, or local pockets of nematic order, are left before the next cooling stage. We have confirmed that 1 h at 170 °C is enough for the polymer chains to equilibrate. Once annealed at 170 °C, the sample was cooled to 80 °C at a rate of 10 °C/min, and an expected exothermic peak was observed at the first-order nematic−isotropic transition at $T_{ni} = 102$ °C on cooling. The temperature was stabilized for 1 min at 80 °C; then it was increased again to 170 °C (at the same rate of 10 °C/min), and the endothermic nematic−isotropic transition peak was recorded on heating. The sample was annealed at 170 °C for 1 h, and then the temperature was again decreased to 80 °C, stabilized at this value for 10 min, and increased to 170 °C. We repeated these cycles in temperature with variable waiting times at 80 °C in the nematic phase of 1, 10, 100, 1000, and 5500 min, shown by the sequence of plots in Figure 4b. Owing to the long annealing time at 170 °C, no variations in the transition features have been noted on cooling; all exothermic peaks are superimposed, Figure 4a, which also gives comfort with respect to thermal and chemical stability of the material over such long periods. On heating the sample, the DSC signal shows one single peak for short waiting times in the nematic phase. However, Figure 4 shows that on increasing the waiting time at 80 °C, this peak splits progressively into two distinct endothermic features. This means that two separate transitions occur when the polymer stays for a time greater than $\sim$1000 min in the nematic phase. This time is consistent with the time necessary for the phase separation to occur in the microscopic observations.

The direct observation of the nematic texture using a polarizing microscope is a convenient tool to study the phase separation in our polydisperse polymers. We present here an analysis of the physical characteristics of the sample, through the evolution of the characteristic size ξ of nematic domains.

Figure 5 shows the time evolution of the average domain size. Before the onset of phase separation, ξ scales as a power law with time, $\xi \approx 0.48 \, t^{1/4}$, to a very good approximation. This effect corresponds to the coarsening of the nematic texture toward a state where the nematic director has a uniform orientation. It is driven by the Frank elasticity of the nematic system and has been reported by many authors in LCP.[8−11] After $\sim$2600 min, the phase separation becomes apparent and macroscopic circular drops of a different texture appear. Figure 5 shows that the average size of the domains does not evolve with time inside these drops, suggesting that in this phase the system has reached a thermodynamical equilibrium. In the outside region, the domain size fluctuates but, for these big values of ξ, the image analysis errors are too large to allow any quantitative analysis. Nevertheless, one could discern from the image in Figure 2b that the texture there is characterized by a much larger length scale.

There may be an issue of discrepancy between the time after which the phase separation becomes evident under the optical microscope and the (somewhat shorter) time required for the two-transition feature of the DSC signal to develop. The delay in the onset of demixing after the quench may be a real physical effect[21] due to an additional viscoelastic resistance of entangled polymers. We would like to keep an open mind about such an effect because our techniques are unable to reliably resolve the processes occurring at early stages of separation. It is likely that the thermal sensitivity of DSC allows one to distinguish between two emerging phases earlier than the sufficient optical contrast between the two textures can be established. However, we cannot tell whether there has been a significant non-trivial delay at the quench temperature 80 °C before the phase separation begins. Instead, we concentrate on the behavior of the two phases at late stages, near the equilibrium.
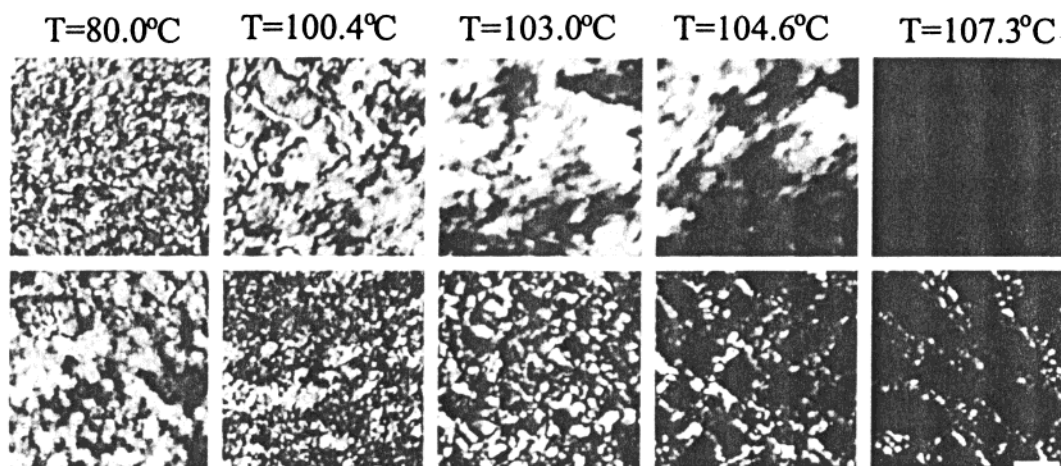
Figure 3. Micrographs of a MCLCP sample between crossed polars, during the increasing of temperature through the nematic–isotropic transition. The rate of heating is 5 °C/min. The initial state corresponds to Figure 2. The top row of images represents the texture evolution inside the drop, and the bottom row corresponds to the outside region. Inside the drops, the transition begins at ~103.6 °C and is completed at 106.0 °C. In the outside region, the transition occurs in a broad zone between 102.5 and 111.0 °C, with a complex morphology. The temperature range of the transition (phase coexistence) is much broader outside than inside the drop. Moreover, the transition appears everywhere at the same time inside the drop, whereas it is discontinuous in the outside region. On the last image, the white bar represents 10 μm.

Starting from the last point of Figure 5, after the polymer has spent 8500 min at 80 °C, we then increase the temperature (at a rate 5 °C/min) up to a value very close to T_{ni} inside the drops, but still in the nematic state. The criteria of how this final temperature is chosen have been described in ref 13; the method uses the average intensity of light transmitted between crossed polars as a estimate of net birefringence and, therefore, the local nematic order $Q(T)$ in the system. At this temperature, the polymer inside the drops is fully in the nematic state, but the nematic–isotropic transition has already begun in the outer phase. Images are recorded, and the domain size can be followed inside and outside the drops. Figure 6 shows that, when increasing the temperature, the domains grow inside the drops. Outside the drop, the domain size does not evolve with temperature. The temperature is then decreased at the same rate to 80 °C. During this last step, domain shrinking is observed inside the drops. The domain size is clearly a reversible function of the temperature in one of the two phases, inside the phase-separated drops in Figure 2.

4. Discussion

Why does the system phase separate, and what are the two emerging phases? In order to answer these questions, we have analyzed the role of added chemical impurities. We have used a series of samples from the same batch, in which a nonmesogenic solvent butylated hydroxytoluene (BHT) has been gradually added, from 0 to 3.42% (by mass). In all these samples the phase separation occurred in exactly the same manner. Figure 5 shows that the time evolution of the average domain size is the same in the polymer where no impurities were added and in the sample where a relatively large amount of chemical impurity, 3.42% BHT, was added (the same result is obtained for intermediate concentrations of BHT as well). We have also checked that the behavior of ξ when varying the temperature was the same in all these doped samples. These observations led us to the conclusion that chemical impurities in the system are not relevant in the observed phase behavior. In the following, we discuss the possibility of a segrega-

tion between long and short polymer chains driven by the establishing nematic order.

In the previous paper,[13] we have studied the evolution of nematic Schlieren textures of the same MCLCP, but with longer chains. No phase separation was observed, and the nematic textures corresponded to a thermodynamically equilibrium (stable or metastable) state of the system. The behavior of the average domain size in response to a temperature change near the nematic–isotropic transition is similar to the behavior reported in the present study, inside the drops (Figure 6). In ref 13 we have attributed this reversible feature to the fact that an essentially fixed concentration of entanglements always exists in the system, quenching some mesogens in a random orientation and introducing disorder to the nematic orientational order. This in particular relates to the MCLCP with chains above their hairpin limit.[22,23] The sketch in Figure 1b illustrates a possible reason for the halted coarsening—the chain relaxation may be completely quenched if the length of rigid rodlike mesogenic unit (say $l \sim 30$ Å) is greater than the reptation tube diameter a, a function of chain contour length Nl (for comparison, this size $a \sim 66$ Å in PMMA[24]). Sufficiently long polymer chains should effectively behave as cross-linked elastomers when in the nematic phase.

The equilibrium texture is then due to the competition between this effectively quenched random disorder and the nematic Frank energy, which penalizes the spatial variations of the director field; see ref 15 for details. The characteristic domain size is $\xi \simeq 16\pi^2 K^2/(\rho_x g^2)$, with K the Frank elastic constant of the nematic, ρ_x the density of quenched impurities, and g the energy of local coupling between such an impurity and the director **n**. Both K and g depend on the temperature T via the nematic order parameter $Q(T)$, which is also the measure of chain anisotropy in MCLCP. Near the transition temperature, the Frank constant scales as $K \sim Q^2$.[1] Because the nematic transition is regarded as only weakly first-order, the near-critical behavior near T_{ni} is often interpolated with an empirical dependence $Q(T) \approx \Delta Q + (1 - T/T_{ni})^\gamma$ [25] with the jump at the transition $\Delta Q \approx 0.4$ and the exponent $\gamma \approx 0.2$. Assuming that the
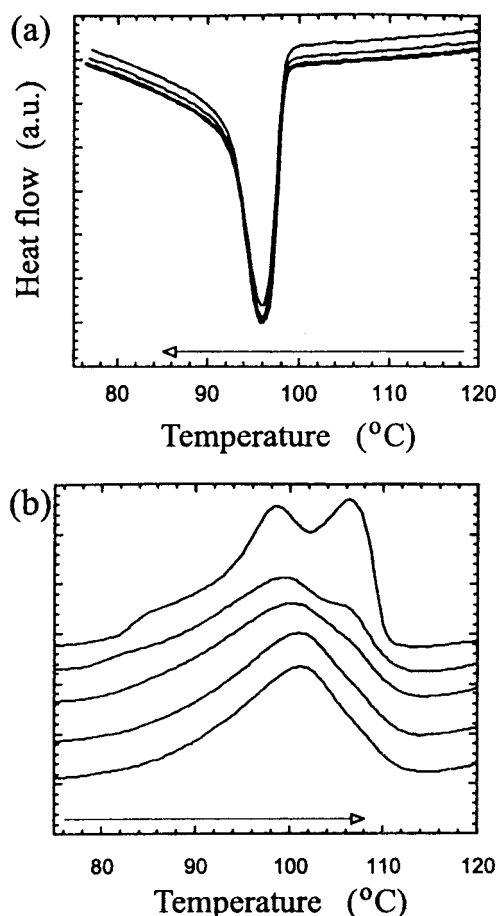
Figure 4. DSC scans on cooling (a) and heating (b) the MCLCP between the nematic state (80 °C) and the isotropic state (170 °C). The rate of heating is 10 °C/min. The polymer is first annealed at high temperature in the isotropic phase and then cooled to 80 °C. The curves correspond to the waiting times of 1, 10, 100, 1000 and 5500 min at 80 °C. Exothermic peaks on cooling (a) superimpose, showing that the system reached its equilibrium in the isotropic state. Endothermic peaks on heating (b), after the polymer has aged for different times in the nematic state before increase of the temperature (see text), show the onset and the subsequent evolution of phase separation. For a short waiting time, one single transition occurs on heating, whereas two separate transitions are increasingly visible when the time spent in the nematic phase is greater than ~1000 min.

coupling constant g scales with order parameter as a power law $g \sim Q^\epsilon$, a fit of the experimental values robustly gives $g \sim Q^3$.[13] Figure 6 shows that in the present study, the fitting of $\xi(T)$ inside the drops of fine texture, using the same simple model, gives the same exponent $\epsilon = 3$. We must reiterate that, although the data points in Figure 6 show the texture size apparently constant between 80 and 100 °C, the fit does provide the power-law exponent relating the size $\xi \propto Q^{-2}$ (which then leads to the said $g \sim Q^3$) when the local order parameter $Q(T)$ is given by the very sharp empirical relation.[25]

The difference between the previous MCLCP studied in ref 13 and the system used in the present study is the average length of the polymer chains: they are much shorter in the present study, but also with high polydispersity. We then interpret the process of phase separation in the following way. In MCLCP of average low molecular weight, the nematic texture coarsens in time as long as the chain length is smaller than a critical length above which entanglements will necessarily
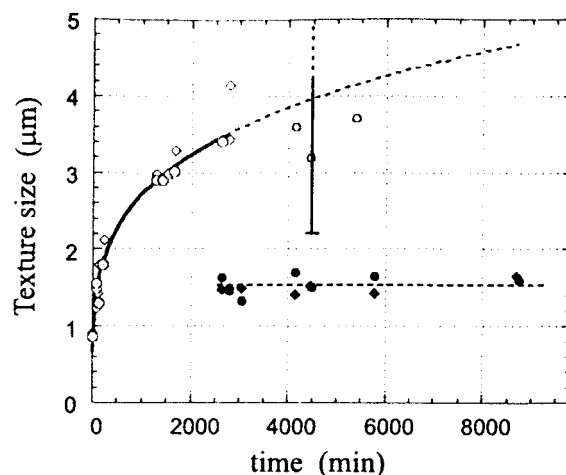

Figure 5. Time evolution of the characteristic domain size. For $0 < t < 2600$ min, the sample is monophase and the texture coarsens with $\xi \simeq 0.48 t^{1/4}$ (solid line). For $t > 2600$ min, the phase separation occurs and circular drops of fine texture are clearly visible in Figure 2. Inside the drops (filled symbols), the domain size ξ stops evolving in time, suggesting that an equilibrium is reached, and is smaller than the scale reached in the coarsened mixture. Outside the drops (open symbols), the texture is coarsened further; the large percolating regions of uniform director, cf. Figure 2b, make the statistical analysis of domains ambiguous (the large error bar is not limited at the top of the plot). The diamond symbols correspond to the original sample, and the circles correspond to the same sample where impurities (3.42% of BHT) have been deliberately added. There is no difference between the two samples.
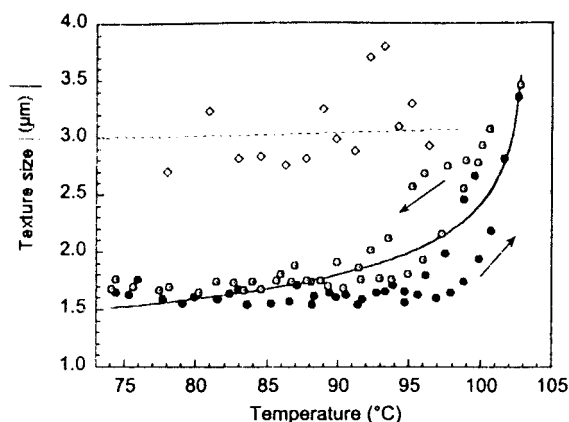

Figure 6. Evolution of the average domain size with temperature. Initially, the sample has waited 8500 min at 80 °C, and the phase separation has occurred. The temperature is then increased at a constant rate of 5 °C/min up to 104 °C (just before the nematic–isotropic transition inside the drops $T_{ni} \simeq 104.5$ °C) filled circles), and decreased back to 80 °C at the same rate (open circles). In the inside region, the domain size varies reversibly when the temperature decreases. Solid line shows the fit of *both* sets of data to the theoretical model presented in ref 13: $\xi \sim K^2/(\rho_x g^2)$ or $\xi \sim \text{const } Q^{4-2\epsilon}$, giving $g \sim Q^3$, the cube of the nematic order parameter, see text and ref 13. The evolution of the average domain size ξ is also measured on increasing the temperature outside the drops (open diamonds): there is no significant variation of ξ on approaching the clearing point.

exist. When the texture coarsens, it evolves always in the same way, with ξ scaling as a power law. In our MCLCP, that corresponds to the behavior of the textures in the preseparated sample (Figure 5). The exact value of the exponent is slightly different for different systems studied over the years, which should be expected because complex effects of polymer viscoelasticity are

at play. In the phase-separated sample, the long chains are inside the drops, the population of shorter chains being left in the continuous phase outside the drops. The textures inside the drops are indeed in a thermodynamical equilibrium, behaving in exactly the same way as those with average large molecular weight.[13] This means that the chains are long enough for a fixed concentration of entanglements to be present in the polymer, stabilizing orientational defects of the director field. At the same time, the shorter chains in the outside regions are not quenched by entanglements, and their Schlieren textures reach quite large domain sizes.

5. Demixing by a Nematic Mean Field

Recently there have been several theoretical attempts to describe the coupling between composition and orientational order in systems involving polymer and liquid crystal components.[26,27] Some of the ideas there are very important, involving the elastic effects of nematic distortions and chain bending, as well as the kinetics of phase evolution. However, we are of the opinion that a simpler description is needed to highlight the effect of phase separation in a system with only one essential chemical component.

We now present such a theoretical argument that explains the observation of phase separation between nematic polymer chains of different molecular weight in our polydisperse system. The idea is similar to several recent models of spinodal decomposition driven by the interaction with an additional ordering field in the system.[28,29] The classical Flory–Huggins model of phase separation[30] considers the competition between the entropy contributions, which favor mixing, and the generic potential energy of "repulsive" interaction between the species that, at appropriate values of the χ-parameter, generates the nonconvex free energy function and resulting instabilities:

$$F \simeq k_B T (\phi \ln \phi + [1 - \phi] \ln[1 - \phi]) + \chi \phi [1 - \phi] \quad (1)$$

The purpose of the present model is to show that a subtle difference in nematic ordering between long and short mesogenic chains can generate a similar destabilizing potential energy contribution to the free energy of our MCLCP, where only one chemical substance is present. Generically, we shall explore the fact that monodisperse chains of different length have different transition temperatures T_{ni} and, therefore, a different nematic order parameter at the same temperature. (Intuitively, the short chains have fewer monomers between the two ends that introduce disorder; thus, their T_{ni} is lower than that for longer chains). In the polydisperse mixture, the order parameter $Q(T)$ is a unique function measuring the mean field experienced by all rodlike mesogenic units, irrespective of which chain they belong to. As a result, each individual chain finds itself out of its optimal nematic conformation and creates a drive to separate from other chains with very different length. Thus a difference in T_{ni} results in an effective repulsive interaction between long and short chains that favors demixing.

To illustrate the point more clearly let us make two specific simplifications:

(1) Assume that our system is a mixture of chains of only *two* lengths, with degrees of polymerization N_1 and N_2, instead of the real continuous spectrum of polydispersity. Then, let us denote the concentration of *mono-*

mers of the first type of chains as ϕ (and, thus, the monomers on the other chain type have $1 - \phi$). Taking into account the degrees of polymerization and neglecting small factors of order $1/N$, the entropy of mixing is, per unit volume

$$S = \frac{k_B}{v_o} \left(\frac{\phi}{N_1} \ln \phi + \frac{1 - \phi}{N_2} \ln[1 - \phi] \right) \quad (2)$$

where v_o is the volume of rodlike monomer.

(2) Assume that the nematic phase transition is described by the second-order mean field Landau expansion of thermodynamic free energy density. In reality, the nematic symmetry requires the transition to be weakly first-order

$$F_n = \frac{1}{2} A_0 [T - T_m(\phi)] Q^2 - \frac{1}{3} BQ^3 + \frac{1}{4} CQ^4 \quad (3)$$

where Q is the value of nematic order parameter and A_0, B, and C are the Landau coefficients whose magnitude is estimated in the Appendix. We shall now take $B \to 0$ to ensure a simpler algebra of the second-order transition. T_m is the mean critical temperature, which is a function of concentration ϕ of the two polymer species in our mixture. If one assumes, in the first approximation, that the nematic transition temperature depends on the length of the polymer chain as $T_c = T_0 + \alpha N$, the mean critical point of the mixture will be

$$T_m = (T_c(1) \phi + T_c(2) [1 - \phi]) = T_c(2) + \alpha(N_1 - N_2)\phi \quad (4)$$

where $T_c(2)$ is the transition temperature of the monodisperse melt of chains with degree of polymerization N_2. Longer chains with fewer ends and greater main-chain correlations have a slightly higher transition point. This effect is firmly established, both experimentally and theoretically,[31] and is also seen in our DSC data, Figure 4, showing a shift of ~5° between two transitions. One could crudely estimate from the literature (e.g., ref 32) $\alpha \sim 0.1$, although it should of course be a complicated function of specific molecular structure.

When the mixture is brought down below the critical point $T_m(\phi)$, the nematic order parameter $Q \neq 0$ and the minimal free energy density (eq 3) of the nematic phase is

$$F_n = -\frac{A_0^2}{4C} [\Delta T + \alpha(N_1 - N_2)\phi]^2 \quad (5)$$

Here the temperature quench $\Delta T = T_c(2) - T$ and $\alpha(N_1 - N_2) \sim 5°$ using eq 4 and the DSC data of Figure 4. The principal feature of this optimized free energy density of a "bidisperse" nematic polymer is the concentration dependence $F_n \propto -\phi^2$, acting in the exact analogy with the χ-term of the Flory–Huggins potential energy.[30] The phase separation into the regions of low-ϕ and high-ϕ concentrations (mainly the chains with degree of polymerization N_2 and N_1, respectively) then proceeds in a similar way as in that classical theory.

This free energy penalty on having the two polymer species uniformly dispersed in the mixture has to be balanced against the entropy of mixing eq 2. The full free energy then becomes

$$\frac{F}{k_B T} v_0 = -\underline{\frac{v_0}{k_B T}\frac{A_0^2}{4C}\alpha^2(N_1 - N_2)^2}\left[\frac{\Delta T}{\alpha(N_1 - N_2)} + \phi\right]^2 +$$

$$\frac{\phi}{N_1}\ln\phi + \frac{1 - \phi}{N_2}\ln[1 - \phi] \quad (6)$$

where the effective demixing potential energy is rearranged from its simplified form for the second-order phase transition, eq 5. The underlined factor in front plays the role of the Flory χ-parameter, its magnitude crucially dependent on the difference in molecular weight between the two polymer species, $(N_1 - N_2)^2$. Obviously, when this difference is greater, the effect of demixing becomes more pronounced. Another parameter, unusual for the classical Flory−Huggins model, is the temperature difference between the nematic transition point and the quench temperature, ΔT. This temperature shift is generally small, compared to the absolute temperature, and may be positive or negative, the latter when the system is cooled below $T_m(\phi)$ but not as far as the lower bound $T_c(2)$. Because the factor $\alpha(N_1 - N_2)$ is of the same order of magnitude as the interval $T_c(1) - T_c(2)$, the argument of the square brackets in F_n, eqs 5 and 6, may be always negative, be always positive, or change its sign at $\phi = \Delta T/\alpha(N_1 - N_2)$. This affects the balance of energy between the two phases and the shape of the free energy plots; see Figure 7a. However, the phase diagrams shown in Figure 7b for two different values of the effective χ-parameter are only weakly affected by the relative position of the nematic−isotropic transition point. In fact, for the simplified second-order transition case expressed in eq 6, the spinodals are completely independent of ΔT.

Finding the spinodal and the critical point ϕ^* is especially straightforward for the quadratic potential energy $F_n(\phi)$:

$$\frac{v_0}{k_B T}\frac{A_0^2}{4C} = \frac{1}{\alpha^2(N_1 - N_2)^2}\left[\frac{1}{N_1\phi} + \frac{1}{N_2(1 - \phi)}\right];$$

$$\phi^* = \frac{\sqrt{N_2}}{\sqrt{N_1} + \sqrt{N_2}} \quad (7)$$

Clearly, the relative position of the critical point of demixing (ϕ^*, T^*) and the nematic transition point $T_m(\phi)$ depends on the difference in molecular weight ($N_1 - N_2$). When $N_1 \approx N_2$, the separation may only start below the absolute temperature $T^* \to 0$. One may estimate the condition when the critical point T^* coincides with the nematic transition point $T_m(\phi^*)$—the situation between the two examples plotted in Figure 7b

$$N_1 - N_2 \approx$$

$$\sqrt{\frac{A_0^2}{4C}\frac{v_0 T_c(2)}{k_B}}\frac{\sqrt{N_1} + \sqrt{N_2}}{\alpha\sqrt{N_1 N_2}} \sim \frac{1}{\alpha N^{1/2}}\sqrt{\left(\frac{A_0^2 T_c^2}{4C}\right)\frac{v_0}{k_B T_c}} \quad (8)$$

the last equation obtained assuming both N_1 and N_2 are large and ignoring the small difference in nematic transition points.

The nematic potential energy part, $F_n(\phi)$, of the effective free energy (eq 6) can be obtained with better accuracy from a correct first-order transition form (eq 3). The qualitative behavior is the same as described
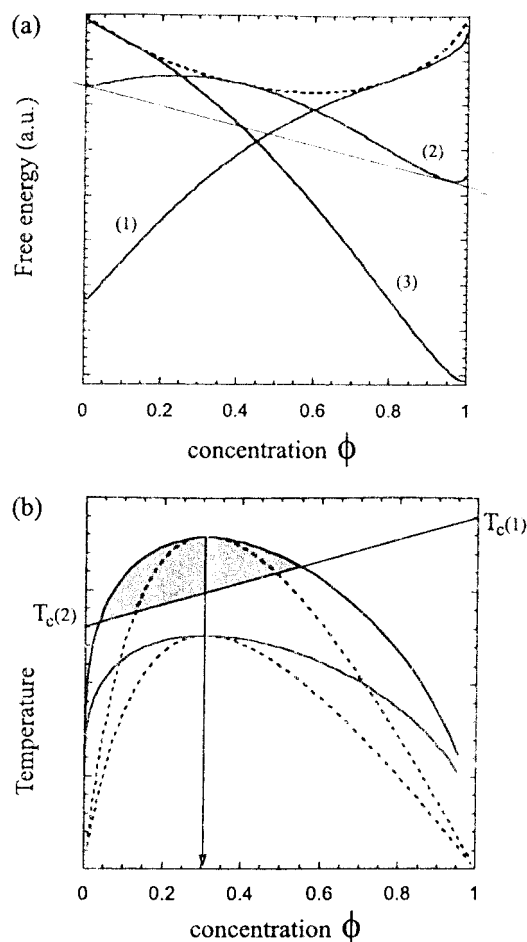
(a)

(b)

Figure 7. Stability analysis for a real first-order transition nematic free energy. The Landau parameters are chosen as described in the Appendix, $N_1 = 25$, $N_2 = 5$, and $\alpha = 0.25$. (a) Plotting the full free energy density eq 6 for a sequence of decreasing values of T: $T > T_c(2)$ curve 1, $T \approx T_c(2)$ curve 2, and $T < T_c(2)$ curve 3. The dashed line is the free energy of isotropic phase $Q = 0$, which allows good mixing. The example common-tangent line is drawn for curve 2. (b) The phase diagram, showing the nematic transition line $T_m(\phi)$ and two sets of spinodal−binodal curves for slightly different numerical values of effective χ-parameter, eq 6. Shading indicates the "virtual" demixing region where the nematic energy above $T_m(\phi)$ is zero and does not compete with the mixing entropy. The arrow shows the critical point ϕ^*, eq 7.

above, although explicit calculation is more tedious. Avoiding this, we simply plotted the numerical results in Figure 7, for the values of Landau coefficients and material parameters estimated in the Appendix.

6. Conclusion

The mean-field analysis of the previous section is a crude approximation of the real nematic transition in main-chain polymers and of the coupling between the orientational order and chain conformations. Other limitations are the treatment of mixture as only a two-component system and the linear dependence of critical temperature on degree of polymerization. However, in spite of these simplifications, the main points outlined here remain valid:

(1) Because there is a variation of transition temperature (and the optimal nematic order parameter Q at a given temperature) with the chain length N, there is a tendency for separating the components with different degrees of polymerization. Each of them could then

reach a deeper minimum of the nematic free energy, which may overwhelm the effect of mixing entropy. The effective demixing parameter is proportional to the square of "polydispersity" $N_1 - N_2$.

(2) In order for the described mechanism to proceed, the polymer melt has to have sufficient mobility. When the chains are too long (as we have seen in ref 13), the motion is effectively frozen and the mixture behaves as an equilibrium polydomain texture. When the chains are too short, in the oligomer region, there is no sufficient difference in the behavior of the phases after separation.[3] (Note that the drive for phase separation might be even stronger for oligomer chains, because the dependence $T_c(N)$ is very steep: parameter α may be as large as 50.) Only in the relatively narrow region of mean degree of polymerization could we expect the described effect to be observed—when the regions of separated long chains will behave in a physically distinct way from the short chains.

This present study shows that in polydisperse MCLCP of low average molecular weight, a phase separation occurs between two phases of slightly different nematic—isotropic transition temperatures. Having checked that the presence of chemical impurities is irrelevant for this effect, and as all the polymers are made of the same monomer, we attribute this difference in clearing temperature to the fact that chains of different length have different nematic order parameters, the short chains being more likely to undergo a transition for smaller temperatures. Analysis of the texture and comparison with previous studies[13] show that long polymer chains tend to group inside circular drops, surrounded by shorter chains. Using a theoretical argument based on the classical Flory—Huggins theory of phase separation, but taking into account the potential energy term associated with the nematic mean field, we demonstrate that the segregation between chains of different molecular weight is induced by the nematic order. Although this mechanism is similar to the well-studied process of phase separation in mixtures made of polymer and low molecular weight liquid crystals, e.g., in forming the polymer-dispersed liquid crystal matrices, the novelty here is the absence of any chemical dissimilarity between the system components, except the length of polymer chains.

Appendix: Landau Parameters for a Nematic Polymer

Over the years, a large number of experiments have been performed to investigate the nematic—isotropic phase transition. It is useful to find the values of the three phenomenological parameters describing the transition, coefficients A_0, B, and C in eq 3. Although different materials will have these parameters slightly different, it is instructive to examine the characteristic orders of magnitude. In order to determine three parameters, one needs three independent measurements. We are fortunate that there are, in fact, four available:

(1) The first measurement could be the jump of order parameter at the weak first-order transition $\Delta Q_{ni} = 2B/3C$. There might be large errors in its determination,

which should depend (among other factors) on the rate of cooling through the transition. However, because Q only varies between 0 and 1 and because a number of molecular theories predict this jump explicitly, one can take qualitatively $Q_{ni} \simeq 0.5$, giving $B \approx 0.75C$.

(2) The second measurement can be the interval between the transition temperature and the critical point T^* (the latter is usually determined by extrapolating the inverse susceptibility, $\chi^{-1} \sim |T - T^*|$). In usual low molar mass liquid crystals, this interval is rather small, but in main-chain polymers one may expect $T_{ni} - T^* \sim 5°$. From the Landau theory, $T_{ni} - T^* = 2B^2/9A_0C$, which gives $B \approx 30A_0 \times 1$ K. (Note that the dimensionality of B and C is energy density, while A_0 has the dimensions of J/m^3 K.)

(3) A third measurement can be the enthalpy of transition $\Delta H = T_{ni}(2A_0B^2/9C^2)$, per unit volume. It is usually obtained from calorimetry by integrating the characteristic DSC peak of the first-order transition. Again, a large uncertainty may accompany such a measurement because at any nonzero cooling rate the conditions are not exactly equilibrium. However, keeping up the qualitative approach, the value of transition enthalpy per unit mass is around ~ 2 J/g at a reasonably slow cooling rate. Taking the density $\rho \sim 1$ g/cm^3 and the $T_{ni} = 380$ K, we obtain

$$A_0 \sim 5 \times 10^4 \, \text{J/m}^3 \, \text{K}$$

$$\text{then} \quad B \sim 1.5 \times 10^6 \quad \text{and} \quad C \sim 2 \times 10^6 \, \text{J/m}^3 \quad (9)$$

(4) It is fortunate that the three measurements above give estimates that agree with the fourth way of accessing A_0. The nematic correlation length is typically determined by the ratio of the bare Frank elastic constant $\kappa = K/Q^2$ to the thermodynamic energy density: $\xi^2 = \kappa/A_0\Delta T$. There are many ways of obtaining the characteristic magnitude of $\xi \sim 10$ nm. Taking a value for the Frank constant of main-chain polymers to be a few times larger than that of low molar weight nematics, $\kappa \sim 5 \times 10^{-11}$ J/m, and $\Delta T \sim 10°$, we obtain $A_0 \sim 5 \times 10^4$ J/m^3 K, in a very reasonable agreement with the previous estimate.

The final unknown parameter in the free energy (eq 6), or its full first-order transition analogue used in numerical plotting, is the mesogenic monomer volume v_0. For the molecule shown in Figure 1a one has, crudely, $v_0 \sim 10^{-26}$ m^3. Then, at around 100 °C ($k_B T \approx 6.5 \times 10^{-21}$ J), the effective χ-parameter underlined in eq 6 is

$$\chi \simeq 5 \times 10^{-4} \alpha^2 (N_1 - N_2)^2$$

References and Notes

(1) de Gennes, P. G.; Prost, J. *The Physics of Liquid Crystals*, 2nd ed; Oxford University Press: New York, 1993.
(2) Chuang, I.; Durrer, R.; Turok, N.; Yurke, B. *Science* **1991**, *251*, 1336.
(3) Chuang, I.; Turok, N.; Yurke, B. *Phys. Rev. Lett.* **1991**, *66*, 2472.
(4) Nagaya, T.; Orichara, H.; Ishibashi, Y. *J. Phys. Soc. Jpn.* **1992**, *61*, 3511.
(5) Gotz, S.; Stille, W.; Strobl, G.; Scheuermann, H. *Macromolecules* **1993**, *26*, 1520.
(6) Doi, M.; Edwards, S. F. *The Theory of Polymer Dynamics*; Clarendon Press: Oxford, 1986.
(7) Long, D.; Morse, D. *Europhys. Lett.* **2000**, *49*, 255.
(8) Noël, C. In *Handbook of Liquid Crystals*; Demus, D., et al., Eds.; Wiley-VCH: Weinheim, Chichester, 1998; Chapter 2.

(9) Hashimoto, T.; Nakai, A.; Shiwaku, T.; Hasegawa, H.; Rojstaczer, S. R.; Stein, R. S. *Macromolecules* **1989**, *22*, 422.

(10) Rieger, J. *Macromolecules* **1990**, *23*, 1545.

(11) Shiwaku, T.; Nakai, A.; Hasegawa, H.; Hashimoto, T. *Macromolecules* **1990**, *23*, 1590.

(12) Rojstaczer, S. R.; Stein, R. S. *Macromolecules* **1990**, *23*, 4863.

(13) Elias, F.; Clarke, S. M.; Peck, R.; Terentjev, E. M. *Europhys. Lett.* **1999**, *47*, 442.

(14) Terentjev, E. M. *J. Phys.: Condens. Matter* **1999**, *11*, R239.

(15) Fridrikh, S. V.; Terentjev, E. M. *Phys. Rev. E* **1999**, *60*, 1847.

(16) Clarke, S. M.; Terentjev, E. M.; Kundler, I.; Finkelmann, H. *Macromolecules* **1998**, *31*, 4862.

(17) Riccardi, C. C.; Borrajo, J.; Williams, R. J. J.; Masood Siddiqi, H.; Dumon, M.; Pascault, J. P. *Macromolecules* **1998**, *31*, 1124.

(18) Nephew, J. B.; Hihei, T. C.; Carter, S. A. *Phys. Rev. Lett.* **1998**, *80*, 3276.

(19) Chiu, H. W.; Kyu, T. *J. Chem. Phys.* **1999**, *110*, 5998.

(20) Percec, V.; Kawasumi, M. *Macromolecules* **1991**, *24*, 6318.

(21) Clarke, N.; McLeish, T. C. B.; Pavawongsak, S.; Higgins, J. S. *Macromolecules*, **1997**, *30*, 4459.

(22) de Gennes, P. G. In *Polymer Liquid Crystals*; Cifferi, A., Krigbaum, W. R., Meyer, R. B., Eds.; Academic Press: New York, 1982; Chapter 5.

(23) Li, M. H.; Brulet, A.; Davidson, P.; Keller, P.; Cotton, J. P. *Phys. Rev. Lett.* **1993**, *70*, 2297.

(24) Fetters, L.; Lohse, D.; Richter, D.; Witten, T.; Zirkel, A. *Macromolecules* **1994**, *27*, 4639.

(25) Halley, I. *Prog. Solid State Chem.* **1975**, *10*, 103.

(26) Fukuda, J.-i. *Phys. Rev. E* **1998**, *58*, R6939.

(27) Matsuyama, A.; Kato, T. *Phys. Rev. E* **1999**, *59*, 763.

(28) Olmsted, P. D.; Poon, W. C. K.; McLeish, T. C. B.; Terrill, N. J.; Ryan, A. J. *Phys. Rev. Lett.* **1998**, *81*, 373.

(29) Tanaka, H. *J. Phys.: Condens. Matter* **1999**, *11*, L159.

(30) Flory, P. J. *Principles of Polymer Chemistry*; Cornell University Press: Ithaca, NY, 1953.

(31) Sigaud, G.; Yoon, D. Y.; Griffin, A. *Macromolecules* **1983**, *16*, 875. Wang, X. J.; Warner, M. *J. Phys. A: Math. Gen.* **1986**, *19*, 2215.

(32) Sirigu, A. In *Liquid Crystallinity in Polymers; Principles and Fundamental Properties* Ciferri, A., Ed.; VCH Publishers: New York, 1991; Chapter 7.